Collaborative Configuration Optimization of Soft Open Points and Distributed Multi-energy Stations with Spatiotemporal Coordination and Complementarity

Shengyuan Wang, Fengzhang Luo, Chengshan Wang, Yunqiang Lyu, Ranfeng Mu, Jiacheng Fo, and Lukun Ge

***Abstract*—To address the limitations of traditional planning methods in handling complex scenarios such as multi-feeder or substation cluster supply under high photovoltaic (PV) penetration, this paper proposes a collaborative configuration optimization method of soft open points (SOPs) and distributed multi-energy stations with spatiotemporal coordination and complementarity to reduce renewable energy curtailment. First, a shared strategy of multiple types of resources is proposed based on an SOP-enabled flexible distribution network. Second, a distributed hydrogen-based multi-energy coupling system (DHMECS) is developed. Then, a DHMECS siting model considering inter-feeder resource sharing is formulated. Finally, a configuration model of SOP and DHMECS is proposed, incorporating a partitioned autonomous operation strategy that considers spatiotemporal coordination and complementarity. The proposed method is validated on the improved Portugal 54-node and 219-node distribution networks, and the results demonstrate that it mitigates severe voltage violations and PV curtailment, enhances partitioned autonomous operation capabilities, and addresses the challenges of complex planning scenarios involving multi-feeder or substation cluster supply.**

***Index Terms*—Spatiotemporal coordination and complementarity, multi-energy station, soft open point, configuration optimization, distribution network, photovoltaic (PV).**

I. Introduction

SINCE the industrial revolution, the large-scale development and utilization of fossil fuels have led to resource depletion, climate change, and environmental pollution. Accelerating the energy transition has become a global consensus [1]. The European Union and China have set their respective carbon neutrality targets for 2050 and 2060 [2]. Distributed photovoltaic (PV), which is critical to renewable energy production and the electrification of energy consumption, has developed on a scale far beyond expectations. In the first half of 2024 alone, China added 52.88 GW of new distributed PV capacity, bringing the total to 310 GW [3]. However, the large-scale integration of high-penetration distributed PV energy has resulted in severe voltage violations [4], uncertain power flow directions [5], and difficulties in source-load matching [6], posing new challenges to the hosting capacity of distribution networks. Efficiently allocating multiple types of resources to explore diversified pathways for distributed PV energy utilization and enhancing the capacity of modern distribution networks to support distributed PV energy remain critical issues that need urgent resolution.

With large-scale integration of high-penetration distributed PV energy, the distribution network faces two core challenges: ① the rigidity of the traditional network topology limits the capability of flexible power transfer, hindering inter-feeder power exchange and leading to the saturation of local absorption capacity; ② the distribution network essentially functions as a foundational platform for enabling spatiotemporal coordination and complementarity of multiple types of resources. However, current technological methods have not fully explored the potential of spatiotemporal coordination and complementarity among multiple types of resources and lack the capability for global optimization of the distribution network.

With large-scale integration of energy resources and increasing demand for flexible resource dispatch, the limitations of the existing radial distribution network topology [7], [8] have become increasingly prominent [9]. Traditional distribution networks are unable to actively control energy flows between feeders, and the effectiveness of resource con-

Manuscript received: December 29, 2024; revised: March 6, 2025; accepted: June 7, 2025. Date of CrossCheck: June 7, 2025. Date of online publication: July 15, 2025.

This work was supported by Smart Grid-National Science and Technology Major Project (No. 2024ZD0800800) and Science and Technology Project of State Grid Corporation of China "Low-carbon and Reliable Urban Power Distribution System Demonstration Project" (No. SGTJDK00DWJS2400298).

S. Wang, F. Luo (corresponding author), C. Wang, R. Mu, and J. Fo are with the State Key Laboratory of Smart Power Distribution Equipment and System, Tianjin University, Tianjin, China (e-mail: wangshengyuan@tju.edu.cn; luofengzhang@tju.edu.cn; cswang@tju.edu.cn; muranfeng@tju.edu.cn; fjc_099@tju.edu.cn).

Y. Lyu is with the State Grid Hebei Electric Power Co., Ltd., Shijiazhuang, China (e-mail: lvyq@he.sgcc.com.cn).

L. Ge is with State Grid Tianjin Electric Power Company, Tianjin, China (e-mail: gelk@tju.edu.cn).

DOI: 10.35833/MPCE.2024.001279

figuration is typically confined to individual feeders, lacking global optimization across feeders [10]. This limitation hinders the spatiotemporal coordination and complementarity among generation, grid, load, and storage across different feeders, thereby reducing the overall operation efficiency and flexibility of the distribution network. With the technical development of power electronics, flexible interconnection devices represented by soft open points (SOPs) and energy routers (ERs) have provided new means and ideas for enhancing the flexibility of grid operation. SOPs are primarily applied between different feeders [11], where they flexibly control power flows across feeders, enabling the sharing of multiple types of resources and improving the flexibility and resource utilization efficiency of distribution networks. Reference [11] points out that SOPs possess capabilities such as feeder load balancing, voltage profile improvement, power loss reduction, three-phase balancing, distributed generation hosting capacity enhancement, and supply restoration, further highlighting their important role in enhancing the flexibility of medium-voltage distribution networks.

The future utilization of PV energy requires deep integration with other industries and promotes a green transition in terminal energy consumption [12] - [14]. Against this backdrop, integrated energy systems (IESs) [15]-[17] can flexibly coordinate multiple energy forms, including electricity, heat, and gas, significantly improving PV utilization rates (PURs) [18], [19]. For example, the distributed microgrid proposed in [20] and the combined heat and power (CHP) model with carbon capture presented in [21] have both demonstrated the potential of IES for optimized operation. However, most of these IESs rely on natural gas as the energy carrier, posing challenges in terms of safety, economic feasibility, and environmental impact [22]. In contrast, hydrogen, as a zero-carbon resource, has attracted significant attention [23] - [25]. For example, [26] indicates that compared with pumped hydro storage and gravity energy storage, distributed hydrogen-based multi-energy systems are more suitable for distribution networks with high PV penetration [25], [27]. Additionally, [28] proposes a hydrogen-based distributed IES that significantly reduces operation costs. However, the existing planning studies on IES with distributed hydrogen generally lack a wide-area resource coordination mechanism at the distribution network level. The applications are mainly limited to individual microgrids or localized regions, making it difficult to accommodate the widespread and dispersed nature of PV deployment in distribution networks. This limitation hinders the deep integration of IES with the distribution network hierarchy and constrains global optimization capabilities, making it challenging to meet the future development needs of zonal autonomy in distribution networks.

To address the aforementioned issues, this paper proposes a collaborative configuration optimization method of SOPs and distributed multi-energy stations with spatiotemporal coordination and complementarity. The contributions of this paper are as follows.

1) To address the issue of flexible resource sharing and coordination across regions in partitioned autonomous systems, a shared strategy of multiple types of resources is proposed based on an SOP-enabled flexible distribution network. By flexibly controlling power flows among feeders through SOP, the dynamic coupling and optimal complementarity of flexible resources across feeders are promoted, thereby enhancing the overall operation efficiency and regulation flexibility of the distribution network.

2) To facilitate the effective utilization of high-penetration distributed PV energy, this paper proposes a DHMECS integrating energy conversion, multi-energy coordination, and spatiotemporal complementarity. By leveraging various energy forms such as cold, heat, and hydrogen, DHMECS enables the conversion, storage, and utilization of curtailed PV energy. Meanwhile, a DHMECS siting model is also proposed.

3) A partitioned autonomous operation strategy is proposed, and a configuration model of SOP and DHMECS is developed to support the evolving needs of future distribution networks in partitioned supply-demand balancing, efficient utilization of distributed PV energy, and autonomous operation.

The remaining sections are as follows. Section II introduces a shared strategy of multiple types of resources based on SOP-enabled flexible distribution network. Section III presents DHMECS siting model with coordination units. Section IV introduces the establishment of the configuration model for SOP and DHMECS. Section V conducts case analysis. Section VI presents the conclusions.

II. Shared Strategy of Multiple Types of Resources Based on SOP-enabled Flexible Distribution Network

A. SOP-enabled Flexible Distribution Network

Future (flexible) distribution networks with high-penetration distributed PV energy face challenges such as voltage violations and large-scale curtailment of PV generation. The traditional unidirectional radial distribution network is no longer adequate. Moreover, traditional expansion planning methods, e. g., constructing new substations and upgrading lines, fail to meet modern requirements [29].

By replacing tie switches with SOPs, the distribution network can be divided into multiple coordination units based on electrical connections, transitioning to an partitioned autonomous operation mode centered on these units. Flexible resources within coordination units can be shared across feeders, enabling a shift in the balancing method of distribution network from source-load balancing at individual feeders to autonomous balancing within coordination units. Figure 1 illustrates the SOP-enabled flexible distribution network and traditional distribution network (with tie switches), where the former supports the sharing of multiple types of resources and partitioned autonomous operation within a region.

B. Establishment of SOP Operation Model

SOP is crucial for energy interaction in multi-feeder operations. Common SOP devices include back-to-back voltage source converter (B2B-VSC) [30], static synchronous series compensator (SSSC) [31], and unified power flow controllers (UPFC) [32].

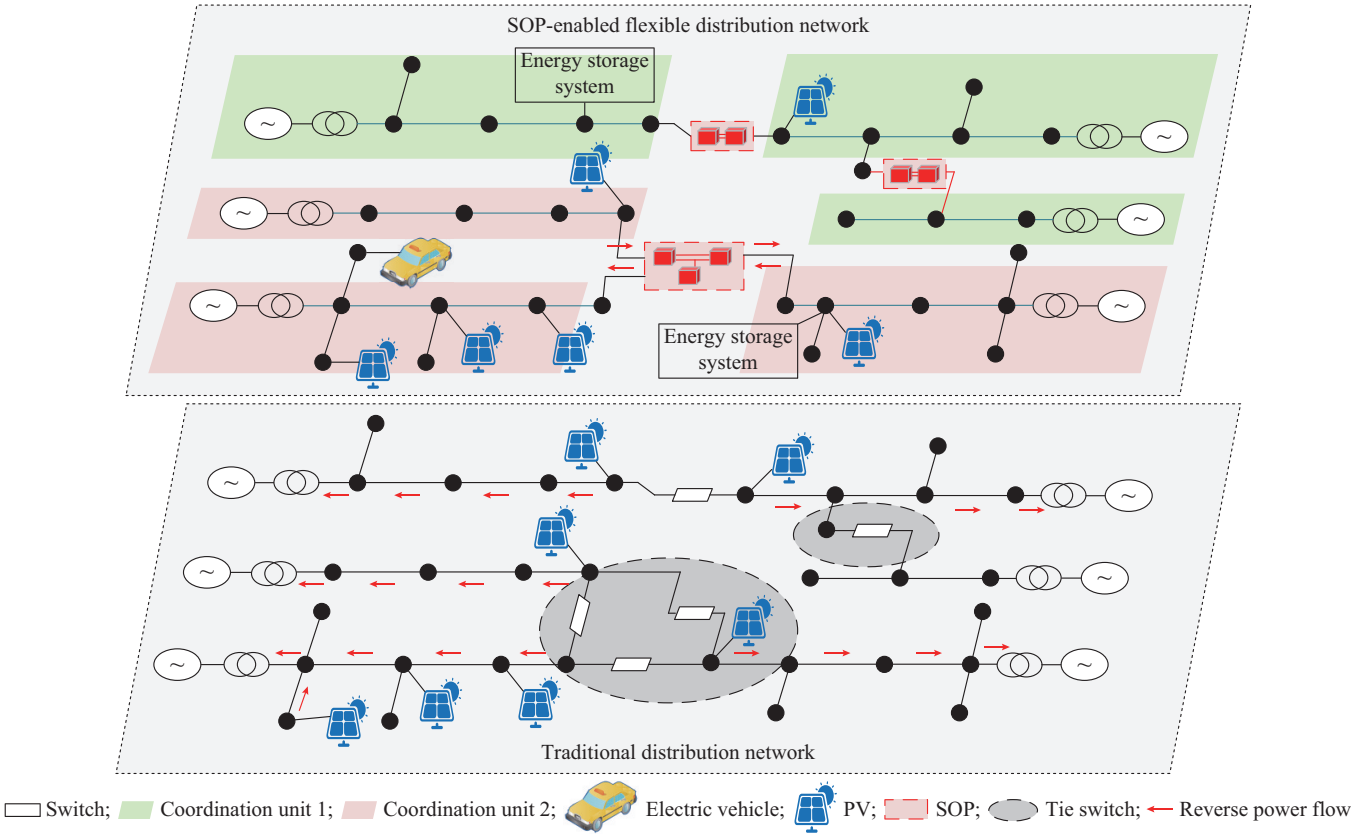

Fig. 1. Illustration of SOP-enabled flexible distribution network and traditional distribution network.

Figure 2 illustrates the circuit topology of the SOP based on B2B-VSC, which primarily consists of two VSCs and a DC capacitor. As shown in the figure, VSC1 and VSC2 are located between two feeders and are interconnected via a DC link to form a bipolar system. Each VSC typically adopts a three-phase bridge circuit composed of insulated gate bipolar transistors (IGBTs) and anti-parallel diodes. This circuit utilizes the DC capacitor for energy buffering and employs an AC filter inductor to reduce output current harmonics.

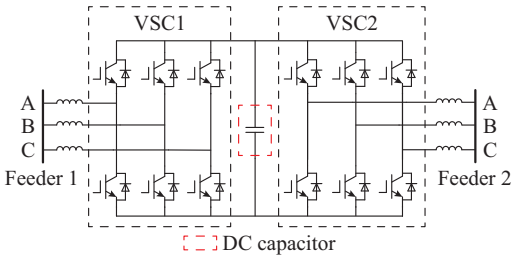

Fig 2. Circuit topology of SOP based on B2B-VSC.

From an operation perspective, the power flow control of the SOP relies on the coordinated operation of both VSCs. Under steady-state operation conditions, the SOP adopts the PQ-$V_{dc}Q$ control mode [30], [33], [34], where one terminal regulates output power while the other controls the DC-side voltage. Each VSC has two control variables (active and reactive power), both of which contribute to the optimal operation of the distribution network. Based on the steady-state model of the SOP, (1) and (2) provide the operation constraint equations for distribution network optimization.

1) Active Power Limits for SOP

$$P_{s,i,t}^{SOP,\phi}=-P_{s,j,t}^{SOP,\phi} \quad \forall s \in \Omega_{SOP} \tag{1}$$

where the subscript t denotes the time interval; $P_{s,i,t}^{SOP,\phi}$ and $P_{s,j,t}^{SOP,\phi}$ are the three-phase active power of nodes i and j connected through the s^{th} SOP, respectively; Ω_{SOP} is the set of SOP devices; and ϕ denotes the three phases.

2) Capacity Constraints for SOPs

$$\sqrt{(P_{s,i,t}^{SOP,\phi})^2+(Q_{s,i,t}^{SOP,\phi})^2} \le S_{s,i}^{SOP,\phi} \tag{2}$$

where $Q_{s,i,t}^{SOP,\phi}$ is the three-phase reactive power of node i connected through the s^{th} SOP; and $S_{s,i}^{SOP,\phi}$ is the capacity of node i connected through the s^{th} SOP.

III. DHMECS Siting Model with Coordination Units

A. DHMECS Energy Conversion

Within the coordination unit, SOP transfers curtailed PV energy from multiple feeders to consumption devices. To efficiently utilize the curtailed PV energy while meeting diverse user demands, this paper proposes the DHMECS energy conversion, as shown in Fig. 3, as an energy aggregation carrier. The specific devices in the DHMECS are as follows: alkaline electrolysis cell (AEC), lithium bromide absorption chiller (LBAC), electric heat pump (EHP), thermal storage tank (TST), hydrogen storage tank (HST), solid oxide fuel cell (SOFC), and electric chiller (EC).

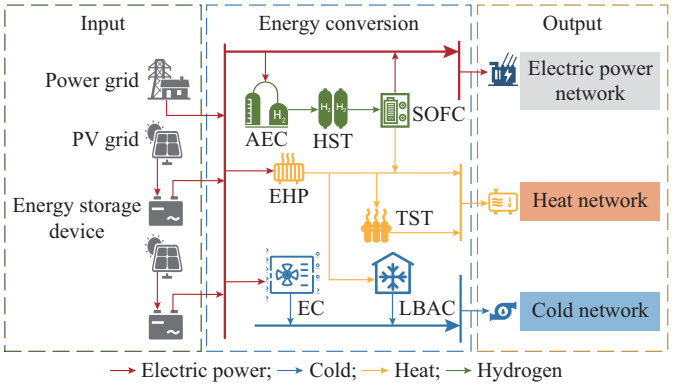

Fig. 3. Schematic diagram of DHMECS energy conversion.

In modeling, DHMECS faces two major challenges: ① the complex coupling of multiple energy forms requires precise balance relationships, and ② multi-energy coordination across temporal dimensions increases modeling complexity [28]. Therefore, the model must fully consider the balance of multiple energy types and the interaction of devices across temporal scales.

1) Electric Power Balance of DHMECS

DHMECS includes three power consuming devices, i.e., EHP, EC, and AEC. The electric power balance equation is:

$$P_{grid}(t)+P_{SOFC,E}(t)+PV(t)=P_{EHP,in}(t)+P_{AEC,in}(t)+P_{EC,in}(t) \quad (3)$$

where $P_{grid}(t)$ is the electric power from the upper-level grid; $P_{SOFC,E}(t)$ is the discharging power of SOFC; $PV(t)$ is the electric power supplied by the PV; $P_{EHP,in}(t)$ is the electric power input to the EHP; $P_{AEC,in}(t)$ is the electric power input to the AEC; and $P_{EC,in}(t)$ is the electric power input to the EC.

2) Heat Power Balance of DHMECS

DHMECS meets the heat power demands within the coordination unit. There are three heat devices of DHMECS, i.e., SOFC, TST, and EHP. The heat power balance equation is:

$$P_h(t)+P_{LBAC,in}(t)+P_{TST,in}(t)=P_{EHP,out}(t)+P_{TST,out}(t)+P_{SOFC,H}(t) \quad (4)$$

where $P_h(t)$ is the heat power supplied to the users in the coordination unit; $P_{LBAC,in}(t)$ is the electric power input to LBAC; $P_{TST,in}(t)$ is the heat power input from TST; and $P_{EHP,out}(t)$, $P_{TST,out}(t)$, and $P_{SOFC,H}(t)$ are the heat power from EHP, TST, and SOFC, respectively.

3) Cold Power Balance of DHMECS

DHMECS meets the cold power demands within the coordination unit. EC and LBAC provide the cold power outputs of DHMECS. The cold power balance equation is:

$$P_c(t)=P_{EC,out}(t)+P_{LBAC,out}(t) \quad (5)$$

where $P_c(t)$ is the cold power required by the coordination unit; $P_{EC,out}(t)$ is the cold power output from EC; and $P_{LBAC,out}(t)$ is the cold power output from LBAC.

B. Mathematical Model of Devices of DHMECS

1) Mathematical Model of AEC

$$P_{AEC,out}(t)=\alpha_{AEC}P_{AEC,in}(t) \quad (6)$$

where $P_{AEC,out}(t)$ is the electric power output from AEC; and α_{AEC} is the energy conversion efficiency of AEC.

2) Mathematical Model of HST

$$E_{HST,in}(t)=P_{AEC,out}(t)\Delta t \quad (7)$$

where $E_{HST,in}(t)$ is the amount of hydrogen input; and Δt is the unit time interval.

$$E_{HST}(t)=E_{HST}(t-1)+\eta_{HST}\beta_{HST}(t)E_{HST,in}(t)-(1-\beta_{HST}(t))E_{HST,out}(t)\frac{1}{\eta_{HST}} \quad (8)$$

where $E_{HST}(t)$ is the amount of hydrogen stored in HST; η_{HST} is the charging/discharging efficiency of HST; β_{HST} is a 0/1 variable that responds to the operation condition of the HST; and $E_{HST,out}(t)$ is the amount of hydrogen output.

$$E_{HST}(0)=E_{HST}(24) \quad (9)$$

where $E_{HST}(0)$ and $E_{HST}(24)$ are the remaining capacities of HST at the first and last moments, respectively.

3) Mathematical Model of SOFC

$$P_{SOFC,E}(t)=\alpha_{SOFC}\frac{E_{HST,out}(t)}{\Delta t} \quad (10)$$

where $P_{SOFC,E}(t)$ is the electric power output from SOFC; and α_{SOFC} is the SOFC conversion efficiency.

$$P_{SOFC,H}(t)=\alpha_{SOFC,H}\theta_{SOFC}P_{SOFC,E}(t) \quad (11)$$

where $\alpha_{SOFC,H}$ is the heat-electric ratio of SOFC; and θ_{SOFC} is the waste heat utilization of SOFC.

4) Mathematical Model of EHP

$$P_{EHP,out}(t)=\alpha_{EHP}P_{EHP,in}(t) \quad (12)$$

where α_{EHP} is the EHP conversion efficiency.

5) Mathematical Model of TST

$$E_{TST}(t)=E_{TST}(t-1)+\eta_{TST}\beta_{TST}(t)E_{TST,in}(t)-(1-\beta_{TST}(t))E_{TST,out}(t)\frac{1}{\eta_{TST}} \quad (13)$$

where $E_{TST}(t)$ is the amount of heat stored in TST; η_{TST} is the charging/discharging efficiency of TST; β_{TST} is a 0/1 variable that responds to the operation condition of the TST; and $E_{TST,in}(t)$ and $E_{TST,out}(t)$ are the amounts of input and output heat power, respectively.

$$E_{TST}(0)=E_{TST}(24) \quad (14)$$

where $E_{TST}(0)$ and $E_{TST}(24)$ are the remaining capacities of the TST at the first and last moments, respectively.

6) EC Mathematical Model

$$P_{EC,out}(t)=\alpha_{EC}P_{EC,in}(t) \quad (15)$$

where α_{EC} is the EC conversion efficiency.

7) Mathematical Model of LBAC

$$P_{LBAC,out}(t)=\alpha_{LBAC}P_{LBAC,in}(t) \quad (16)$$

where α_{LBAC} is the LBAC conversion efficiency.

C. Selection of Critical Nodes Within Coordination Units

Voltage violations are prominent in active distribution networks. DHMECS not only meets diverse energy demands within coordination units but also provides voltage support for deployment nodes. This paper builds on the voltage sensitivity from [35] and reduces the computational complexity

through simplification, extending its application from single-feeder node selection to node selection of coordination unit. The DHMECS siting model comprehensively considers node voltage sensitivity, deviation magnitude, temporal and operation scenario weights, and the resource-sharing characteristics within coordination units.

1) A voltage offset weighting factor is introduced into the traditional voltage sensitivity, reflecting the upward and downward differential voltage regulation needs of different nodes. The sensitivity $S_{mn,t}$ of the voltage at node m to the change in active power injected at node n can be expressed as:

$$S_{mn,t}=\lambda_{mn,t}\Delta V_{m,t} \tag{17}$$

$$\Delta V_{m,t}=V_{m,t}-V_{eu,m,t} \tag{18}$$

where $\lambda_{mn,t}$ is the traditional voltage sensitivity index; $\Delta V_{m,t}$ is the desired voltage deviation; $V_{m,t}$ is the current node voltage; and $V_{eu,m,t}$ is the node desired voltage.

2) The comprehensive sensitivity $S_{m,t}$ of node m with respect to its feeder is:

$$S_{m,t}=\left|\sum_{m\in\Phi_{FL}}\lambda_{mn,t}\Delta V_{m,t}\right| \tag{19}$$

where Φ_{FL} is the set of load nodes of the current feeder.

3) In the time dimension, different time periods are assigned different weights, and the comprehensive sensitivity $S_{op,m,t}$ of the weights of node m is given as:

$$S_{op,m,t}=\sum_{t=1}^{24}S_{m,t}(N_{exceed,t}+1)\max(|V_{exceed,t}|) \tag{20}$$

where $N_{exceed,t}$ is the number of voltage violation nodes; and $V_{exceed,t}$ is the voltage violation value.

4) By assigning different weights to different operation conditions according to the number of days under different operation conditions, e. g., different seasons, the combined sensitivity $S_{opw,m}$ of the weights under different operation conditions is introduced as:

$$S_{opw,m}=\sum_{op=1}^{M}S_{op,m,t}D_{ays,op} \tag{21}$$

where M is the number of types of operation conditions; and $D_{ays,op}$ is the number of days under different operation conditions.

5) Within a coordination unit, the resource sharing between feeders is feasible, and the calculation results of nodes within the unit must be ranked to serve as the basis for DHMECS siting. For a distribution network containing R coordination units, each coordination unit and its internal nodes are sorted, and the sorted index is:

$$I_r=sort(\{S^r_{opw,m}\})\quad \forall m\in\Omega^{r,node},\forall r\in\Omega^R \tag{22}$$

where $\Omega^{r,node}$ is the set of all load nodes within the coordination unit r; and Ω^R is the set of coordination units.

IV. Establishment of Configuration Model of SOP and DHMECS

A. Objective Function and Constraints

The objective function C encompasses the investment cost of various devices C_{inv}, maintenance cost of various devices C_{main}, network loss cost C_{loss}, PV curtailment cost C_{apv}, and DHMECS revenue C_m. Among these, C_m has a significant impact on the operation interaction between DHMECS and SOP. C_{inv} needs to be converted into an equivalent annual value using the capital recovery factor (CRF). The derivation of CRF can be found in [36], and its application in distribution network planning is discussed in [26].

$$C=\min(C_{inv}+C_{main}+C_{loss}+C_{apv}+C_m) \tag{23}$$

$$C_{inv}=\sum_{i\in\Psi}(CRF_i\cdot c_i^{inv}P_e^i) \tag{24}$$

$$\Psi=\{\text{AEC, HST, SOFC, EHP, TST, EC, LBAC, SOP}\} \tag{25}$$

$$CRF=\frac{(1+r)^{LT}r}{(1+r)^{LT}-1} \tag{26}$$

$$C_{main}=\sum_{i\in\Psi}c_i^{main}P_e^i \tag{27}$$

$$C_{loss}=\sum_{op=1}^{M}\sum_{t=1}^{24}\sum_{mn\in\Omega_{line}}D_{ays,op}f_{loss,t}r_{mn}I^2_{mn,t} \tag{28}$$

$$C_{apv}=\sum_{op=1}^{M}\sum_{t=1}^{24}\sum_{pv\in\Omega_{pv}}D_{ays,op}P^{op}_{pv,t}f_{pv} \tag{29}$$

$$\begin{aligned}C_m=\sum_{op=1}^{M}\sum_{t=1}^{24}D_{ays,op}[&P_{grid}(t)\lambda_t^{grid}\Delta t-(\lambda_t^{ele}P_{SOFC,E}(t)\Delta t+\\&\lambda_t^{heat}P_h(t)\Delta t+\lambda_t^{cold}P_c(t)\Delta t)]\end{aligned} \tag{30}$$

where CRF_i is the CRF of the i^{th} device; Ψ is the set of devices; r is the interest rate; LT is the device lifespan; c_i^{inv} is the investment cost of the i^{th} device; P_e^i is the rated power/capacity of the i^{th} device; c_i^{main} is the maintenance cost of the i^{th} device; op is the number of scenarios; r_{mn} is the line resistance; Ω_{line} is the set of lines; $D_{ays,op}$ is the number of days in scenario op; $f_{loss,t}$ is the TOU price; $I^2_{mn,t}$ is the square of the line current of line mn; Ω_{pv} is the set of PVs; $P^{op}_{pv,t}$ is the curtailed PV energy; f_{pv} is the unit curtailment cost; λ_t^{grid} is the purchasing price of TOU; λ_t^{ele} is the selling price of TOU; λ_t^{heat} is the selling price of heat power; and λ_t^{cold} is the selling price of cold power.

The specific constraints of the above objective function are as follows:

1) Operation Constraints of Distribution Network

$$\begin{aligned}\sum_{i\in\pi(:,j)}(P_{ij,op,t}-r_{ij}I^2_{ij,op,t})=&P^{net}_{j,op,t}-\eta_{dh}P^{DH}_{j,op,t}+\\&\eta_{sop}P^{SOP}_{j,op,t}+\sum_{k\in\delta(j,:)}P_{jk,op,t}\end{aligned} \tag{31}$$

$$\sum_{i\in\pi(:,j)}(Q_{ij,op,t}-x_{ij}I^2_{ij,op,t})=Q^{net}_{j,op,t}+\eta_{sop}Q^{SOP}_{j,op,t}+\sum_{k\in\delta(j,:)}Q_{jk,op,t} \tag{32}$$

where $\pi(:,j)$ is the set of end nodes; $\delta(j,:)$ is the set of starting nodes; $P_{ij,op,t}$ and $Q_{ij,op,t}$ are the active and reactive power flowing through the branch ij, respectively; $P^{net}_{j,op,t}$ is the net load of the node; $I^2_{ij,op,t}$ is the square of current of branch ij; η_{dh} and η_{sop} denote whether the node is connected to DHMECS and SOP, respectively; $P^{DH}_{j,op,t}$ is the power of DHMECS; and $P_{jk,op,t}$ and $Q_{jk,op,t}$ are the outgoing active and re-

active power from the current node to the child node, respectively.

$$U_{j,op,t}^2 = U_{i,op,t}^2 + (r_{ij}^2 + x_{ij}^2) I_{ij,op,t}^2 - 2(r_{ij} P_{ij,op,t} + x_{ij} Q_{ij,op,t}) \quad (33)$$

$$I_{ij,op,t}^2 U_{i,op,t}^2 - P_{ij,op,t}^2 - Q_{ij,op,t}^2 = 0 \quad (34)$$

where $U_{j,op,t}^2$ and $U_{i,op,t}^2$ are the squares of the voltage magnitudes of nodes j and i, respectively; and $P_{ij,op,t}^2$ and $Q_{ij,op,t}^2$ are the squares of the active and reactive power through the branch ij, respectively.

$$\begin{cases} 0 \le I_{ij,op,t}^2 \le I_{ij,\max}^2 \\ U_{i,\min}^2 \le U_{i,op,t}^2 \le U_{i,\max}^2 \end{cases} \quad (35)$$

where $I_{ij,\max}^2$ is the square of the maximum current that the branch ij can withstand; $U_{i,\max}^2$ and $U_{i,\min}^2$ are the squares of the upper and lower node voltage limits, respectively; and $U_{i,op,t}^2$ is the square of the current node voltage.

2) Operation Constraints of Devices of DHMECS

The operation constraints of devices of DHMECS have been defined in (3)-(16).

3) Operation Constraints of SOP

The operation constraints of SOP are defined in (1) and (2).

4) Operation Constraints of Coordination Unit

$$P_{dh,discharge,n} \le P_{net,n} \quad \forall P_{net,n} > 0, \forall n \in \{1, 2, \ldots, N\} \quad (36)$$

where $P_{dh,discharge,n}$ is the net discharging power of all DHMECS in the n^{th} coordination unit; and $P_{net,n}$ is the net load of the n^{th} coordination unit.

C. Second-order Cone Optimization

The constraints (2) and (34) contain quadratic terms, leading to nonlinearity and strong non-convexity in the model, making it difficult to solve directly. Therefore, this paper uses a second-order cone optimization algorithm to reformulate constraints (2) and (34). The reformulated forms are:

$$\left\| \begin{matrix} P_{s,i,t}^{SOP,\phi} \\ Q_{s,i,t}^{SOP,\phi} \end{matrix} \right\|_2 \le S_{s,i,t}^{SOP,\phi} \quad (37)$$

$$\left\| \begin{matrix} 2P_{ij,op,t} \\ 2Q_{ij,op,t} \\ I_{ij,op,t}^2 - U_{i,op,t}^2 \end{matrix} \right\|_2 \le I_{ij,op,t}^2 + U_{i,op,t}^2 \quad (38)$$

After replacing (2) and (34) with (36) and (37), the model can be formulated as a mixed-integer second-order cone programming (MISOCP) problem. At this point, the commercial solver CPLEX can be directly used to solve the problem.

V. Case Analysis

A. Description of Test System

This paper is validated on an improved Portugal 54-node distribution network [37], which comprises four substations (S1-S4), ten feeders, and five tie switches. The five tie switches are located at lines 8-33, 9-22, 13-43, 38-39, and 46-47. The SOP locations selected in this paper correspond to the locations of the five tie switches. The improved Portugal 54-node distribution network is shown in Fig. 4. After configuring the SOP devices, the distribution network containing 54 nodes can be naturally divided into three coordination units and two isolated feeders with nodes 21 and 28 as the terminal nodes (not flexibly interconnected with any feeder). As discussed in Sections II and III, the unutilized PV energy within each coordination unit will be flexibly transmitted to DHMECS through SOPs. DHMECS can convert this energy into various forms, i.e., cold, heat, hydrogen, to meet the diverse needs of users within the coordination units. Therefore, based on the principle of proximity, the feeder with node 21 as the terminal node is assigned to coordination unit 1, and the feeder with node 28 as the terminal node is assigned to coordination unit 2.

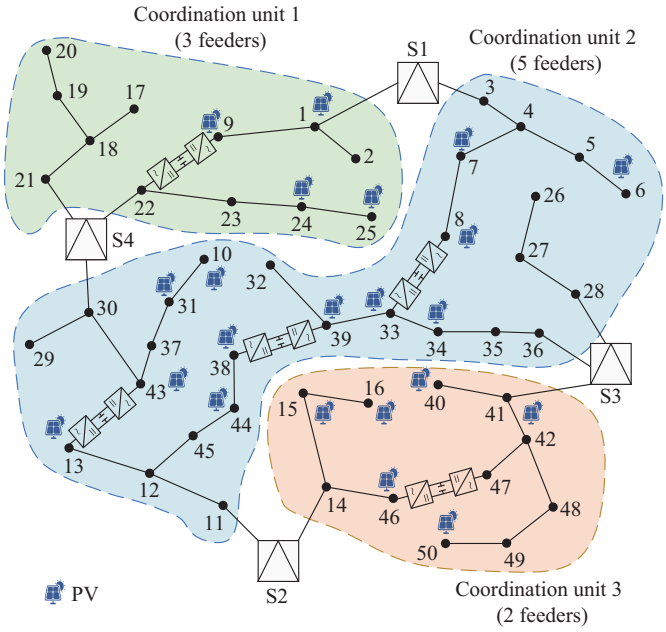

Fig. 4. Improved Portugal 54-node distribution network.

The load data were sourced from the distribution network of a city in northern China, spanning from September 2022 to October 2023 (8760 hours). The PV data were generated using the refined physical model chain (PVlib) [20]. The required meteorological data correspond to the same region as the load data. The principles of PVlib can be found in [20]. The primary data for heat and cold power loads came from [38].

In this paper, only the distribution network is planned. DHMECS links the distribution network with the cold/heat networks [26]. We assume that, for each coordination unit, the ratio of its cold/heat power demand to the total cold/heat power demand is equal to the ratio of its electric power demand to the total power demand. Table I presents the cost parameters related to each device.

TABLE I
Cost Parameters Related to Each Device

Parameter	Value	Parameter	Value
α_{AEC}	0.75	c_{LBAC}^{inv}	1200 ¥/kW
α_{SOFC}	0.6	c_{EHP}^{inv}	1920 ¥/kW
α_{EHP}	4	c_{TST}^{inv}	185.17 ¥/kWh
α_{EC}	3.8	c_{HST}^{inv}	106.5 ¥/kWh
α_{LBAC}	1.3	c_{SOFC}^{inv}	4450 ¥/kW
θ_{SOFC}	0.88	c_{EC}^{inv}	970 ¥/kW
c_{SOP}^{inv}	1000 ¥/kVA	c_{AEC}^{inv}	2210 ¥/kVA

Table II presents the TOU price. The unit heat price is 0.223 ¥/kWh [26]. The operation limits for voltage safety are ±0.05 p.u.. Furthermore, when DHMECS utilizes the existing surplus PV energy, no payment is required for this portion of electricity.

TABLE II
TOU PRICE

Time period	Price (¥/kWh)
11:00-15:00, 19:00-22:00	1.08
08:00-10:00, 16:00-18:00	0.73
01:00-07:00, 23:00-24:00	0.36

Models in planning problems are often complex, and the computational efficiency is therefore critical. According to [39], the scenarios are divided based on seasonal operation characteristics. Typical days are selected using *K*-means clustering. The three selected typical scenarios represent the transition season, summer, and winter. Additionally, the scalability in this paper is similar to that in [40], allowing typical days to be replaced without extensive changes. In Table III, the silhouette coefficient (SC) and the Calinski-Harabasz index (CHI) are presented, determining 3 as the optimal cluster number.

TABLE III
DETERMINATION OF CLUSTER NUMBER

Cluster number	SC	CHI
2	0.48	208.63
3	0.57	308.43
4	0.52	238.78
5	0.47	231.20

B. DHMECS Siting Considering Resource-sharing Characteristics

Figure 5 shows the temporal voltage sensitivity of each node. There are two main reasons why DHMECS needs to be deployed in a distributed manner rather than being concentrated in one location. Since the coordination units can transfer energy spatially across feeders, only a few coordination units of DHMECS are required to handle the unutilized PV energy centrally. Additionally, DHMECS should be deployed in a distributed manner to avoid deploying at adjacent nodes, which could lead to resource waste and system redundancy. DHMECS not only provides voltage support for its nodes but also supports nearby nodes. For example, DHMECS installed at node 50 absorbs PV energy through devices like EHP when the voltage exceeds the upper limit and discharges the energy via SOFC when the voltage falls below the lower limit, providing voltage supports to node 50 and the adjacent node 49. Therefore, based on the above principles and the results of Fig. 5, this paper selects nodes 8, 13, 25, 38, and 50 as the DHMECS installation nodes to ensure the efficient resource utilization.

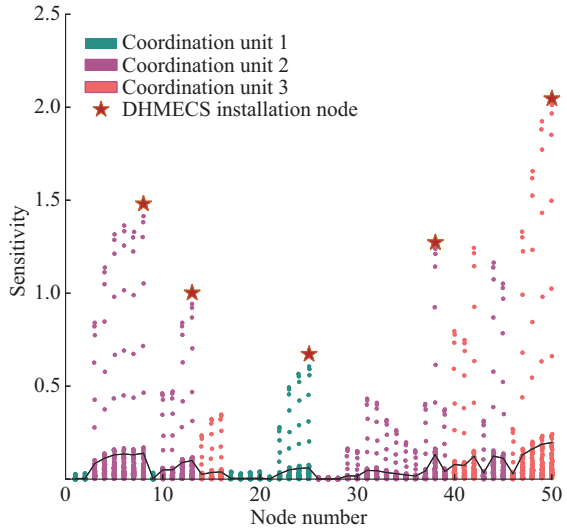

Fig. 5. Temporal voltage sensitivity of each node.

C. Result Analysis

Numerous studies have shown that deploying PV energy consumption devices on a single feeder is effective. However, the existing method heavily depends on land resources and lacks energy interaction between feeders within coordination units, limiting the spatiotemporal regulation capacity of the distribution network. Therefore, this paper enhances network flexibility and PUR by leveraging resource sharing between feeders. To this end, three cases are set in this paper. ① Case 1 considers the energy spatial transfer within the coordination units and hydrogen-based multi-energy flow coupling. SOP and DHMECS are deployed. ② Case 2 considers the energy spatial transfer within the coordination units and electrochemical energy storage (EES). SOP and EES are deployed. The EES is deployed at the same nodes as the DHMECS. The unit investment cost of EES is 1150 ¥/kWh. ③ Case 3 considers the energy spatial transfer within the coordination units. Only SOPs are deployed.

1) Comparative Analysis

Table IV presents indicators for three cases. Specifically, both case 1 and case 2 achieve 100% PUR, indicating that the SOP-enabled flexible distribution network and intra-regional resource-sharing configuration can effectively enhance PUR. Nevertheless, case 1 yields higher annual revenue than case 2, attributed to its diversified energy sales as well as lower investment and maintenance costs. Table V presents the optimal configuration of device capacity and power for DHMECS in case 1. Table VI shows the optimal configuration of SOP capacity in case 1.

TABLE IV
INDICATORS FOR THREE CASES

Case	$C_{inv}+C_{main}$ (10^4 ¥)	C_{loss} (10^4 ¥)	C_m (10^4 ¥)	Annual revenue (10^4 ¥)	PUR (%)
1	1056.171	115.344	2731.568	1560.053	100.00
2	1764.619	84.385	2244.876	395.872	100.00
3	79.863	106.409		186.272	69.29

TABLE V
OPTIMAL CONFIGURATION OF DEVICE CAPACITY AND POWER FOR DHMECS IN CASE 1

Coordination unit	EHP power (kW)	TST capacity (kWh)	SOFC power (kW)	AEC power (kW)	HST capacity (kWh)	EC power (kW)	LBAC power (kW)
1	1899.97	28131.54	54.96	317.37	1225.12	197.87	1303.78
2	4773.35	75346.81	1138.38	3917.32	27093.30	1158.88	3666.82
3	2493.63	37474.89	293.80	1231.93	6992.33	386.99	1855.63
Total	9166.95	140953.25	1487.14	5466.62	35310.75	1743.74	6826.22

TABLE VI
OPTIMAL CONFIGURATION OF SOP CAPACITY IN CASE 1

Line	SOP capacity (MVA)
9-22	1.44
8-33	1.43
38-39	0.65
46-47	2.61
13-43	2.03

Figure 6 shows the heat balance of coordination unit 1 in case 1, where the SOFC output in coordination unit 1 is not prominent. Figure 7 shows the cold balance of coordination unit 1 in case 1 and Fig. 8 shows the SOFC output of node 8 in coordination unit 2. In Fig. 8, a node with a more distinct SOFC output, i.e., node 8 in coordination unit 2, is selected for display.

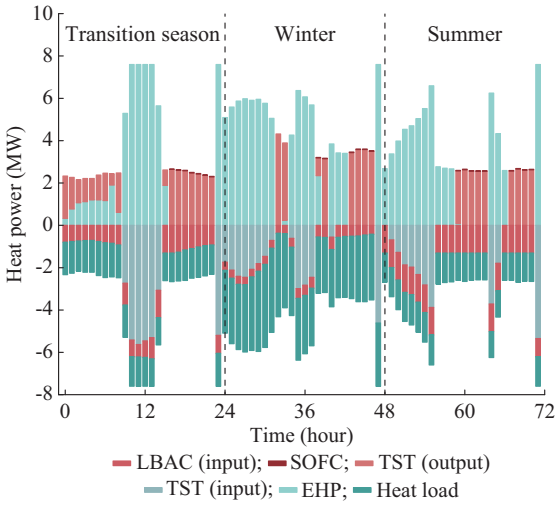

Fig. 6. Heat balance of coordination unit 1 in case 1.

Considering the operation costs, EHPs primarily operate during periods of low electricity prices and high PV output. Energy storage devices, e.g., TST and HST, store energy during these periods and supply it when electricity prices are high, enabling time shifting of energy use. SOFC operates mainly during periods of high electricity price and non-peak PV generation. LBAC acts as the primary cold power device due to economic efficiency. Using DHMECS and SOP devices, the cross-time-space regulation and energy conversion of PV energy are realized, significantly enhancing distributed PUR.

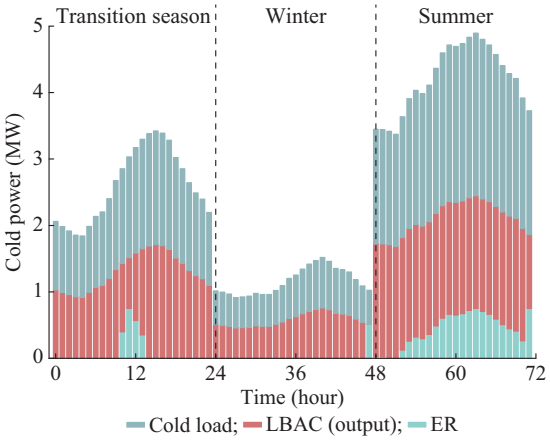

Fig. 7. Cold balance of coordination unit 1 in case 1.

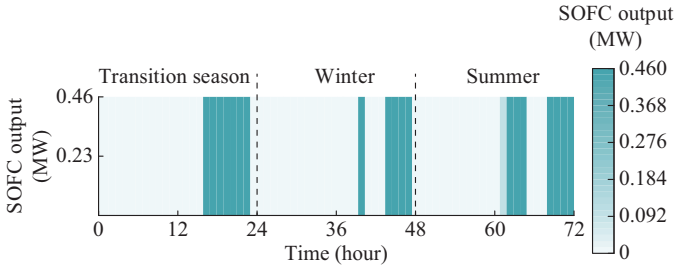

Fig. 8. SOFC output of node 8 in coordination unit 2.

2) Comparison of DHMECS with EES

Energy fluctuations within DHMECS and EES can be compared through the coefficient of variation (CV). Comparative results are shown in Table VII. Table VIII presents the optimal configuration of EES capacity in case 2. HST can interact with cold, heat, and electric power devices. Compared with EES, HST offers more stable energy fluctuations and a lower CV, since PV energy can be converted through multiple paths, with electricity to hydrogen conversion being just one of them. In contrast, EES relies on a single path, limiting the flexibility.

TABLE VII
CV FOR HST AND EES

Coordination unit	CV for HST	CV for EES
1	0.27	0.46
2	0.24	0.47
	0.26	0.48
	0.24	0.49
3	0.24	0.43

TABLE VIII
OPTIMAL CONFIGURATION OF EES CAPACITY IN CASE 2

Coordination unit	EES capacity (kWh)
1	11730
2	50830
3	20480

The cost effectiveness of case 1 is mainly due to two factors. ① In case 1, excess PV energy is stored as hydrogen and heat power. Compared with EES in case 2, the unit investment cost of hydrogen and heat storage is lower. ② Although case 1 introduces more energy coupling devices, these devices do not need to accumulate electric power like the EES in case 2. Instead, the electric power is efficiently converted by the devices and is used for cold and heat power demands, enabling immediate usage. Therefore, the synergy of multiple energy devices reduces the overall investment cost and enhances energy sales revenue through efficient energy conversion, significantly improving the economic efficiency of PV energy handling.

3) Performance Analysis of SOP-enabled Flexible Distribution Network

The SOP-based distribution network facilitates resource sharing across feeders, reducing resource redundancy and land usage. In addition, to further validate the optimization effect of SOP on the distribution network, Table IX presents the optimization results with and without SOP. The optimization with SOP ensures that all node voltages are maintained within the range of 0.95-1.05 p.u., with no voltage violations observed. C_{loss} is reduced by 10.77%, and the maximum voltage deviation decreases by 34.21%. The node voltage on a typical day with SOP is shown in Fig. 9.

TABLE IX
OPTIMIZATION RESULTS WITH AND WITHOUT SOP

Optimization result	C_{loss} (10^4 ¥)	The maximum voltage deviation (p.u.)
Without SOP	119.250	0.076
With SOP	106.409	0.050

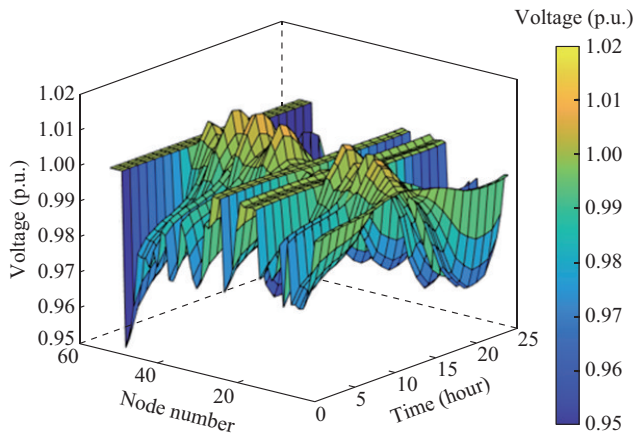

Fig. 9. Node voltage on a typical day with SOP.

Meanwhile, the above discussion primarily focuses on the operation optimization of the distribution network under normal operation conditions. In addition, distribution networks with SOP also demonstrate strong fault recovery capabilities. Compared with traditional tie switches, SOP not only provides continuous power control but also offers voltage support, effectively expanding the supply restoration range and enhancing the load recovery level. Detailed comparisons of the supply restoration performance between SOP and traditional tie switches can be found in [41]. More detailed grid-connected control strategies for SOP can be found in [34] and [42].

D. Evaluation of Proposed Method in a Larger-scale Distribution Network

To verify the applicability of the proposed method in larger-scale distribution networks, we conduct tests on a real-world 10 kV distribution network with 219 nodes in northern China, as shown in Fig. 10, where F1-F15 represent the 15 feeders. The load data from the improved Portugal 54-node distribution network are scaled accordingly, resulting in the peak load of 50.55 MW and the PV penetration rate of 48.89%. Based on time-series voltage sensitivity analysis, the DHMECS sitings are selected at nodes 12, 67, 100, 118, 161, 186, and 217, while the SOPs are set at lines 12-37, 49-67, 57-65, 74-100, 85-99, 118-142, 161-172, 186-199, and 197-217.

According to Table X, both case 1 and case 2 achieve full PV energy utilization. However, case 1 demonstrates superior economic performance. Tables XI and XII further illustrate the optimal configuration of capacity and power of DHMECS and SOP capacity in case 1, respectively, where PV energy is prioritized for immediate conversion into cold and heat power supplies. The remaining energy is stored in low-cost TST and HST, reducing total investment costs while increasing annual revenue. In contrast, case 2 relies solely on EES, leading to higher investment costs. These results confirm that the proposed method remains applicable in larger-scale distribution networks.

By employing a unified mathematical modeling framework, the proposed method can automatically optimize the capacities of various devices to adapt to the characteristics of the target distribution network, requiring only the replacement of network topology information, multi-energy load profiles, and designated SOP/DHMECS node configuration. In addition, since the proposed method incorporates heat and cold, it is particularly well suited for areas with cold and heat power demands, such as urban regions and industrial parks, demonstrating its generality.

VI. CONCLUSION

This paper proposes a collaborative configuration optimization method of SOPs and distributed multi-energy stations with spatiotemporal coordination and complementarity. The main conclusions of this paper are as follows:

1) A shared strategy of multiple types of resources is proposed based on an SOP-enabled flexible distribution network.

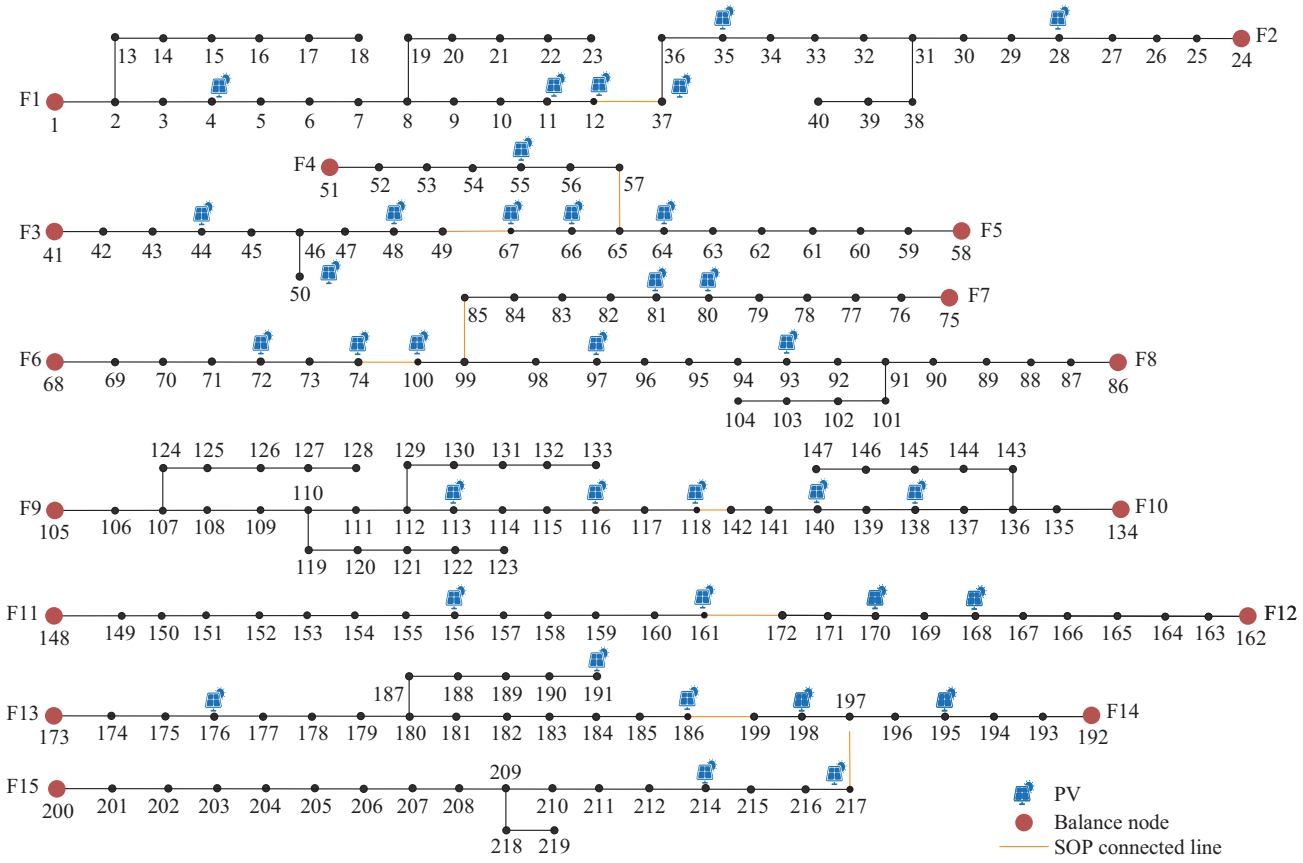

Fig. 10. Structure of 219-node distribution network.

TABLE X
ECONOMIC ANALYSIS FOR CASE 1 AND CASE 2 IN 219-NODE DISTRIBUTION SYSTEM

Case	$C_{inv}+C_{opm}$ (10^4 ¥)	C_{loss} (10^4 ¥)	C_m (10^4 ¥)	Annual revenue (10^4 ¥)	PUR (%)
1	2079.17	154.36	5118.05	2884.52	100
2	3679.02	141.05	4569.51	749.43	100

The limitations of traditional planning methods are addressed in complex scenarios such as multi-feeder group power supply. Specifically, the use of SOP alone reduces network loss costs by 10.77% and decreases the maximum voltage deviation by 34.21%; meanwhile, it reduces the required number of coordination units of DHMECS, thereby significantly improving resource utilization efficiency.

TABLE XI
OPTIMAL CONFIGURATION OF CAPACITY AND POWER FOR DHMECS IN CASE 1

Coordination unit	EHP power (kW)	TST capacity (kWh)	SOFC power (kW)	AEC power (kW)	HST capacity (kWh)	EC power (kW)	LBAC power (kW)
Coordination unit 1 (F1-F2)	2050.97	32222.61	606.34	3096.22	13327.47	506.68	1475.84
Coordination unit 2 (F3-F5)	2684.59	42264.86	746.42	2502.07	17735.93	658.17	2082.51
Coordination unit 3 (F6-F8)	2719.36	42678.15	916.41	3013.16	20979.80	674.42	2133.92
Coordination unit 4 (F9-F10)	2020.41	31725.64	653.90	2094.55	15208.12	500.10	1582.37
Coordination unit 5 (F11-F12)	1941.23	30378.94	752.62	2267.22	16935.89	486.46	1539.19
Coordination unit 6 (two DHMECSs) (F13-F15)	3068.28	48407.98	754.83	2591.70	17965.19	746.33	2361.46

2) DHMECS converts curtailed PV energy into terminal usable energy, meeting diverse energy demands. Compared with EES, DHMECS offers economic advantages: the unit investment costs of HST storage and TST storage are lower than those of EES. Besides, DHMECS enables real-time energy use through power conversion, eliminating the need for large-scale energy accumulation or high-capacity storage devices, further reducing costs.

3) A partitioned autonomous operation strategy based on the collaboration between SOP and DHMECS is proposed, resulting in a configuration model for SOP and DHMECS. This model addresses the shortcomings of existing methods in cross-energy flow and cross-space resource coordination, promotes deep integration and global optimization of multi-energy flow systems and multi-feeder networks, and meets the future needs of distribution networks for partitioned autonomous consumption.

TABLE XII
OPTIMAL CONFIGURATION OF SOP CAPACITY IN CASE 1

Node	SOP capacity (MVA)
12-37	1.78
49-67	2.51
57-65	0.66
74-100	1.00
85-99	1.62
118-142	1.82
161-172	1.86
186-199	1.09
197-217	0.88

In future research, we can further develop a hybrid probabilistic interval method for source load uncertainty modeling to enhance the robustness of planning results, and further investigate methods for efficient PV energy utilization through coordinated operation among distribution networks and microgrids based on ER.

REFERENCES

[1] L. De La Peña, R. Guo, X. Cao *et al.*, "Accelerating the energy transition to achieve carbon neutrality," *Resources Conservation and Recycling*, vol. 177, p. 105957, Feb. 2022.

[2] L. Sun, H. Cui, and Q. Ge, "Will China achieve its 2060 carbon neutral commitment from the provincial perspective?" *Advances in Climate Change Research*, vol. 13, no. 2, pp. 169-178, Apr. 2022.

[3] National Energy Administration. (2024, Jul.). The transcript of the press conference of the National Energy Administration in the first half of 2024. [Online]. Available: http://www.nea.gov.cn/2024-07/31/c_1310783380.htm

[4] X. Sun, J. Qiu, and J. Zhao, "Optimal local volt/var control for photovoltaic inverters in active distribution networks," *IEEE Transactions on Power Systems*, vol. 36, no. 6, pp. 5756-5766, Nov. 2021.

[5] A. Kharrazi, V. Sreeram, and Y. Mishra, "Assessment techniques of the impact of grid-tied rooftop photovoltaic generation on the power quality of low voltage distribution network – a review," *Renewable and Sustainable Energy Review*, vol. 120, p. 109643, Jan. 2020.

[6] Q. Shi, P. Yang, B. Tang *et al.*, "Active distribution network type identification method of high proportion new energy power system based on source-load matching," *International Journal of Electrical Power & Energy Systems*, vol. 153, p. 109411, Nov. 2023.

[7] A. Selim, S. Kamel, and F. Jurado, "Efficient optimization technique for multiple DG allocation in distribution networks," *Applied Soft Computing*, vol. 86, p. 105938, Jan. 2020.

[8] A. Ali, M. U. Keerio, and J. A. Laghari, "Optimal site and size of distributed generation allocation in radial distribution network using multi-objective optimization," *Journal of Modern Power Systems and Clean Energy*, vol. 9, no. 2, pp. 404-415, Mar. 2021.

[9] F. R. Islam, K. Prakash, K. A. Mamun *et al.*, "Aromatic network: a novel structure for power distribution system," *IEEE Access*, vol. 5, pp. 25236-25257, Feb. 2017.

[10] F. Luo, X. Wu, S. Wang *et al.*, "Multi-stage optimization for urban snowflake distribution networks considering spatial-temporal uncertainty and feeder load balancing," in *Proceedings of 2024 IEEE PES General Meeting (PESGM)*, Seattle, USA, Jul. 2024, pp. 1-5.

[11] X. Jiang, Y. Zhou, W. Ming *et al.*, "An overview of soft open points in electricity distribution networks," *IEEE Transactions on Smart Grid*, vol. 13, no. 3, pp. 1899-1910, May 2022.

[12] A. Q. Al-Shetwi, "Sustainable development of renewable energy integrated power sector: trends, environmental impacts, and recent challenges," *Science of the Total Environment*, vol. 822, p. 153645, May 2022.

[13] Y. Gao and A. Qian, "Research on demand side response strategy of multi-microgrids based on an improved co-evolution algorithm," *CSEE Journal of Power and Energy Systems*, vol. 7, no. 5, pp. 903-910, Sept. 2021.

[14] Y. Gao and A. Qian, "A novel optimal dispatch method for multiple energy sources in regional integrated energy systems considering wind curtailment," *CSEE Journal of Power and Energy Systems*, vol. 10, no. 5, pp. 2166-2173, Sept. 2022.

[15] P. Mancarella, "MES (multi-energy systems): an overview of concepts and evaluation models," *Energy*, vol. 65, pp. 1-17, Feb. 2014.

[16] J. Wu, J. Yan, H. Jia *et al.*, "Integrated energy systems," *Applied Energy*, vol. 167, pp. 155-157, Apr. 2016.

[17] Y. Gao, A. Qian, X. He *et al.*, "Coordination for regional integrated energy system through target cascade optimization," *Energy*, vol. 276, p. 127606, Aug. 2023.

[18] F. Ren, Z. Wei, and X. Zhai, "A review on the integration and optimization of distributed energy systems," *Renewable and Sustainable Energy Review*, vol. 162, p. 112440, Mar. 2022.

[19] Z. Zhang, R. Jing, J. Lin *et al.*, "Combining agent-based residential demand modeling with design optimization for integrated energy systems planning and operation," *Applied Energy*, vol. 263, p. 114623, Apr. 2020.

[20] W. Wang, D. Yang, N. Huang *et al.*, "Irradiance-to-power conversion based on physical model chain: an application on the optimal configuration of multi-energy microgrid in cold climate," *Renewable and Sustainable Energy Reviews*, vol. 161, p. 112356, Jun. 2022.

[21] M. Chen, H. Lu, X. Chang *et al.*, "An optimization on an integrated energy system of combined heat and power, carbon capture system and power to gas by considering flexible load," *Energy*, vol. 273, p. 127203, Jun. 2023.

[22] G. Pan, W. Gu, Y. Lu *et al.*, "Optimal planning for electricity-hydrogen integrated energy system considering power to hydrogen and heat and seasonal storage," *IEEE Transactions on Sustainable Energy*, vol. 11, no. 4, pp. 2662-2676, Oct. 2020.

[23] A. Z. Arsad, M. A. Hannan, A. Q. Al-Shetwi *et al.*, "Hydrogen energy storage integrated hybrid renewable energy systems: a review analysis for future research directions," *International Journal of Hydrogen Energy*, vol. 47, no. 39, pp. 17285-17312, May 2022.

[24] M. Yue, H. Lambert, E. Pahon *et al.*, "Hydrogen energy systems: a critical review of technologies, applications, trends and challenges," *Renewable and Sustainable Energy Reviews*, vol. 146, p. 111180, Aug. 2021.

[25] H. Abid, J. Thakur, D. Khatiwada *et al.*, "Energy storage integration with solar PV for increased electricity access: a case study of Burkina Faso," *Energy*, vol. 230, p. 120656, Sept. 2021.

[26] N. Huang, X. Zhao, Y. Guo *et al.*, "Distribution network expansion planning considering a distributed hydrogen-thermal storage system based on photovoltaic development of the whole county of China," *Energy*, vol. 278, p. 127761, Sept. 2023.

[27] A. Emrani, A. Berrada, and M. Bakhouya, "Optimal sizing and deployment of gravity energy storage system in hybrid PV-wind power plant," *Renewable Energy*, vol. 183, pp. 12-27, Jan. 2022.

[28] J. Liu, Z. Xu, J. Wu *et al.*, "Optimal planning of distributed hydrogen-based multi-energy systems," *Applied Energy*, vol. 281, p. 116107, Jan. 2021.

[29] R. Wang, H. Ji, P. Li *et al.*, "Multi-resource dynamic coordinated planning of flexible distribution network," *Nature Communication*, vol. 15, no. 1, p. 4576, May 2024.

[30] Z. Yin, S. Wang, and Q. Zhao, "Sequential reconfiguration of unbalanced distribution network with soft open points based on deep reinforcement learning," *Journal of Modern Power Systems and Clean Energy*, vol. 11, no. 1, pp. 107-119, Jan. 2023.

[31] Y. Chen, D. Wang, J. Li *et al.*, "A SSSC optimal configuration method to enhance available transfer capability considering multi-wind farm access," *IET Renewable Power Generation*, vol. 17, no. 16, pp. 3777-3792, Dec. 2023.

[32] M. Yan, M. Shahidehpour, A. Paaso *et al.*, "A convex three-stage SCOPF approach to power system flexibility with unified power flow controllers," *IEEE Transactions on Power Systems*, vol. 36, no. 3, pp. 1947-1960, May 2021.

[33] L. Bai, T. Jiang, F. Li *et al.*, "Distributed energy storage planning in soft open point based active distribution networks incorporating network reconfiguration and DG reactive power capability," *Applied Energy*, vol. 210, pp. 1082-1091, Jan. 2018.

[34] W. Cao, J. Wu, N. Jenkins *et al.*, "Operating principle of soft open points for electrical distribution network operation," *Applied Energy*, vol. 164, pp. 245-257, Feb. 2016.

[35] Z. Li, S. Chen, Y. Fu *et al.*, "Optimal allocation of energy storage in active distribution networks based on time-sequence voltage sensitivity," *Proceedings of the CSEE*, vol. 37, no. 16, pp. 4630-4640, Aug. 2017.

[36] E. P. DeGarmo, W. G. Sullivan, J. A. Bontadelli *et al.*, "Principles of money-time relationships and applications of money-time relationships," in *Engineering Economy*, Upper Saddle River: Prentice-Hall, 1997, pp. 63-177.
[37] R. Cheng, Z. Xu, H. Li *et al.*, "Distributed energy storage planning in distribution network considering uncertainties of new energy and load," in *Proceedings of 2023 5th Asia Energy and Electrical Engineering Symposium (AEEES)*, Chengdu, China, Mar. 2023, pp. 1364-1369.
[38] Arizona State University. (2024, Jan.). Campus metabolism. [Online]. Available: http://cm.asu.edu/ttps://cm.asu.edu/
[39] Y. Wang, A. O. Rousis, and G. Strbac, "A three-level planning model for optimal sizing of networked microgrids considering a trade-off between resilience and cost," *IEEE Transactions on Power Systems*, vol. 36, no. 6, pp. 5657-5669, Nov. 2021.
[40] C. Gu, Y. Liu, J. Wang *et al.*, "Carbon-oriented planning of distributed generation and energy storage assets in power distribution network with hydrogen-based microgrids," *IEEE Transactions on Sustainable Energy*, vol. 14, no. 2, pp. 790-802, Apr. 2023.
[41] P. Li, J. Ji, H. Ji *et al.*, "Self-healing oriented supply restoration method based on the coordination of multiple SOPs in active distribution networks," *Energy*, vol. 195, p. 116968, Mar. 2020.
[42] M. Yang, X. Pei, and Y. Li, "Multi-port coordinated control strategy of sop in distribution network," in *Proceedings of 2020 IEEE Applied Power Electronics Conference and Exposition (APEC)*, New Orleans, USA, Mar. 2020, pp. 2333-2337.

Shengyuan Wang received the B.S. and M.S. degrees in electrical engineering from Northeast Electric Power University, Jilin, China, in 2020 and 2023, respectively. He is now a Doctoral Student in Tianjin University, Tianjin, China. His research interests include active distribution system planning and decision-making.

Fengzhang Luo received the B.S., M.S., and Ph.D. degrees in electrical engineering from Tianjin University, Tianjin, China, in 2003, 2006, and 2010, respectively. He is currently an Associate Professor with the School of Electrical and Information Engineering, Tianjin University. His main research interests include active distribution system planning and decision-making, and artificial intelligence application in power system.

Chengshan Wang received the Ph.D. degree in electrical engineering from Tianjin University, Tianjin, China, in 1991. Currently, he is a Professor with the School of Electrical and Information Engineering, Tianjin University, where he is also the Director of the Key Laboratory of Smart Grid of the Ministry of Education. He is an Academician of Chinese Academy of Engineering. His current research interests include distribution system analysis and planning, distributed generation system and microgrid, and power system security analysis.

Yunqiang Lyu received the Ph.D. degree in electrical engineering from Texas A&M University, Texas, USA, in 2001. Currently, he is a Chairman with the State Grid Hebei Electric Power Co., Ltd., Shijiazhuang, China. His research interests include distribution system planning and power system security analysis.

Ranfeng Mu received the B.S. degree in electrical engineering from Tianjin University, Tianjin, China, in 2024, where he is now pursuing the M.S. degree. His research interests include active distribution system planning and operation.

Jiacheng Fo received the B.S. degree in electrical engineering from Tianjin University, Tianjin, China, in 2023, where he is now pursuing the M.S. degree. His research interests include active distribution system planning and reliability analysis.

Lukun Ge received the B.S. degree in biomedical engineering from Tianjin University, Tianjin, China, in 2015, the M.S. degree in power energy systems from Cardiff University, Cardiff, UK, in 2016, and the Ph.D. degree in electrical engineering from Tianjin University, in 2024. He is currently working at the State Grid Tianjin Electric Power Company, Tianjin, China. His research interests include reliability and resilience assessment of power systems.